ROYAL SOCIETY
OF CHEMISTRY

PAPER

Check for updates

Synthesis, column packing and liquid chromatography of molecularly imprinted polymers for the acid black 1, acid black 210, and acid Brown 703 dyes†

Faiz Ali, [ID] *[a] Zuber Shah,[a] Alamgir Khan,[a] Maria Saadia,[a] Zeid A. AlOthman [ID] [b] and Won Jo Cheong[c]

Molecularly imprinted polymers have been synthesized for the acid black 1, acid black 210, and acid brown 703 dyes using methacrylic acid, ethylene glycol, and azobisisobutyronitrile as the monomer, cross-linker, and initiator, respectively, in the ratio of 1 : 10 : 44 (template:monomer:cross-linker). The MIPs were used for the selective removal of their corresponding dyes. The selective nature of the MIPs towards their respective dyes was confirmed by a homemade liquid chromatography system. The resultant polymer materials were packed in a stainless steel column and checked for the separation of mixtures of dyes in liquid chromatography. The dyes complementary in structure to the imprinted cavities in the MIPs had long retention times, showing the highly selective nature of the MIPs. The pH, quantity of the MIPs, time, and concentration of the dyes were optimized for the highly efficient removal of the newly synthesized MIP adsorbents in batch adsorption studies. First-order, second-order, and intra-particle diffusion models were applied to all the three MIP-based adsorbents for their kinetic investigations towards the dyes. All the three MIPs selectively absorbed their target template molecule in the presence of four other template dyes having closely related structures with % RSD < 4% for the three batch experiments. The synthesized MIPs were characterized by FTIR, SEM imaging and liquid chromatography. FTIR results strongly confirmed the presence of hydrogen bonding interactions (600–900) between the template and the individual monomers present in the unwashed MIPs. Liquid chromatography revealed the highly selective nature of the MIPs towards their template molecules. The synthesized polymeric substances possess excellent thermal, chemical, and mechanical stability and can be reused several hundred times. The MIPs were applied in the removal of dyes from spiked water samples (river water, tap water and distilled water) where the % removal of the dyes by their corresponding MIPs was greater than 90%.

1. Introduction

The intense colouring materials in dyes chemically interact with certain substrates, imparting more or less permanent colour to the materials.[1,2] These substances absorb the radiation of visible light in a specific wavelength range (400–700 nm).[3,4] Of the two components of the dye, the chromophore is responsible for the dye colour, while the auxochrome intensifies/deepens the colouring effect of the chromophore.[5,6] To improve the aesthetics of products, various synthetic dyes have been widely used as colorants in several chemical industries and household items such as leather, paper, cosmetics, plastics, hair colorants, textiles, and many other industrial products.[7,8] Unfortunately, the exact volume and number of synthetic dyes being produced worldwide are not known.[9] The estimated number of tons of various dyes reported in different articles is approximately 7×10^5 to 1×10^6 per annum around the globe, out of which more than 60% are azo dyes.[8,10,11] The textile industry is the largest consumer of synthetic dyes. Nearly 50% of the dyes consumed by the textile industry are lost during the dyeing processes, while 10–15% of the absorbed dye is released as effluents.[10] The discharge/disposal of industrial dye effluents imparts different colours to the receiving water bodies, which are highly visible and undesirable.[12] The immense scale of production, extensive applications of the synthetic dyes, and improper management can lead to critical environmental pollution and are serious health-risk factors.[9] Dyes present in even minute concentrations in water diminish/prevent light penetration, which results in

[a]Department of Chemistry, University of Malakand, Chakdara Dir(L), 18800, Khyber Pakhtunkhwa, Pakistan. E-mail: faizy186@gmail.com

[b]Department of Chemistry, College of Science, King Saud University, Riyadh 11451, Saudi Arabia

[c]Department of Chemistry, Inha University, 100 Inharo, Namku, Incheon 402-751, South Korea

RSC Advances

View Article Online

Paper

retarded photosynthetic activities, hampers the growth of the biota and makes drinking water unfit for human consumption.[12,13] In addition, dye-contaminated water results in mutagenic and carcinogenic effects and may cause serious physiological changes associated with different disorders such as dysfunctions of the hepatic system, reproductive system, kidneys, brain and central nervous system (CNS).[14–16]

Various dyes (basic dyes, azo dyes, reactive dyes, acid dyes, sulfur dyes, vat dyes, disperse dyes, direct dyes, mordant dyes) are used in different industries. The acid dyes are commonly applied in the textile industry (nylon, silk, angora, and wool) in the pH range of 3–7. Metal complexes are usually present in the structures of acid dyes. Acid dyes are good in their action under acidic conditions in the presence of formic or acetic acid.[17] Being the sodium/ammonium salts of carboxylic, sulfonic, or phenolic organic acids, the acid dyes are highly soluble in aqueous media where the molecules of acid dyes exist in the form of negative charges. Acid dyes can lead to various health issues including allergic dermatitis, irritation of the skin, cancer, and mutations in humans.[18] The reduction in the penetration of light into different water bodies leading to the retarded photosynthesis process in plants is another problem of the dyes.[19] These issues have currently resulted in the removal of acid dyes becoming a critical research area.

Due to the complex structure and synthetic origin, many of the dyes are difficult to degrade since they are generally stable to the various oxidizing agents, photodegradation, biodegradation, and aerobic digestion.[20,21] Therefore, the removal of dyes from water and wastewater before discharging into the environment is very crucial.[21]

Various methods and technologies have been reported, which are commonly employed for the protection of water bodies from different dyes. The different strategies, which are biological, physical, and chemical in nature, have their advantages and shortcomings. However, the complex nature of the effluent, high cost and disposal issues of the residuals diminishes the applicability of many of those conventional methods being used for the treatment of the dye-contaminated water.[22]

Although the biological processing strategies are cost-effective in comparison to the physical and chemical processing strategies, certain commercial dyes are harmful to some microbes. In addition, the biological processes need large areas of land and are time consuming.[6] Similarly, the chemical processing strategies such as coagulation/flocculation and conventional oxidation used for the removal of various dyes from water are often expensive, associated with disposal challenges, and might result in secondary pollution due to the consumption of chemicals.[6,22] The adsorption process is one of the promising techniques used for the effective extraction of the dyes from effluents.[7] The commercially available activation-treated carbon is a good adsorbent material due to the enhanced surface area and high adsorption capacity, and it is commonly used in wastewater treatment.[7,22,23] However, the disposal issues, high cost, non-selectivity, and ineffectiveness against some of the dyes outclass the activated carbon as an adsorbent material.[22,24] It is

therefore imperative to use advanced techniques that are effective and economically cheap for the identification and removal of toxic dyes.[24]

Being one of the most effective, selective, and efficient techniques, molecular imprinting is a widespread approach.[25–27] The ease of the synthesis protocol for polymeric porous materials with high sensitivity and selectivity for the adsorption of small and specific molecules owing to the memory effect at low interference levels makes the MIP approach one of the best approaches.[28–30] These polymeric substances are prepared because of the polymerization of the functional and cross-linking monomers in the presence of template/imprinting molecules.[31–34]

Generally, the non-covalent interactions/attachments are favoured over covalent bonding during the MIPs synthesis. The removal of the non-covalently bound imprinting molecule from the polymer is easy in comparison to the covalently bonded monomers and template molecule in the MIP polymer.[35] At the end of the polymerization, the template molecule is leached out of the polymer, leaving behind the cavities that are complementary in shape and size to the template molecule.[35,36] Owing to the striking features of the MIPs, they have been extensively applied in various fields including solid phase extraction (SPE), chromatographic separations, sensors, membrane technology, environmental monitoring, clinical analysis, medical diagnostics, chiral separation of the pharmaceutically active compounds, and catalysis.[36–43] With the aid of MIP technology, endocrine-disrupting compounds (EDCs) and pesticides have been successfully removed from water and quantified by the repetitive use of the MIP-based adsorbent materials.[39,44] Many advantages offered by the MIPs prepared for different antibodies and natural receptors include excellent operational and storage stabilities, ease of manufacturing and comparatively low prices for material preparation.[45–47]

This project focuses on the synthesis of MIP-based adsorbents for dyes (acid black 1, acid black 210, and acid brown 703) as the template molecules. The MIPs for these dyes have been synthesized for the first time and reported herein. The newly synthesized MIPs have been evaluated for the removal of the dyes both from their respective solutions and from the mixture of solutions containing all three dyes along with other dyes during batch adsorption studies. The adsorption efficiency, regeneration capability, sensitivity, and selectivity of all the three MIPs were found to be very attractive. The synthesized polymeric substances possess excellent thermal, chemical, and mechanical stabilities and can be reused up to hundreds of times. A liquid chromatography system has been developed in our laboratory for studying the high selectivity of the MIPs. The MIPs were packed in different columns of the same dimensions and examined for the separation of a mixture of the dyes containing the target dye for each MIP. Chemical structures, molecular weights, and wavelengths of maximum adsorption for the dyes (acid black-1, acid black-210, acid brown-703, acid black-234, and basic blue-3) are given in Fig. 1. The aim of synthesizing these dye-specific MIPs is to selectively remove the dyes from different industrial effluents with their MIP. The efficiencies of the MIPs synthesized in this project in terms of
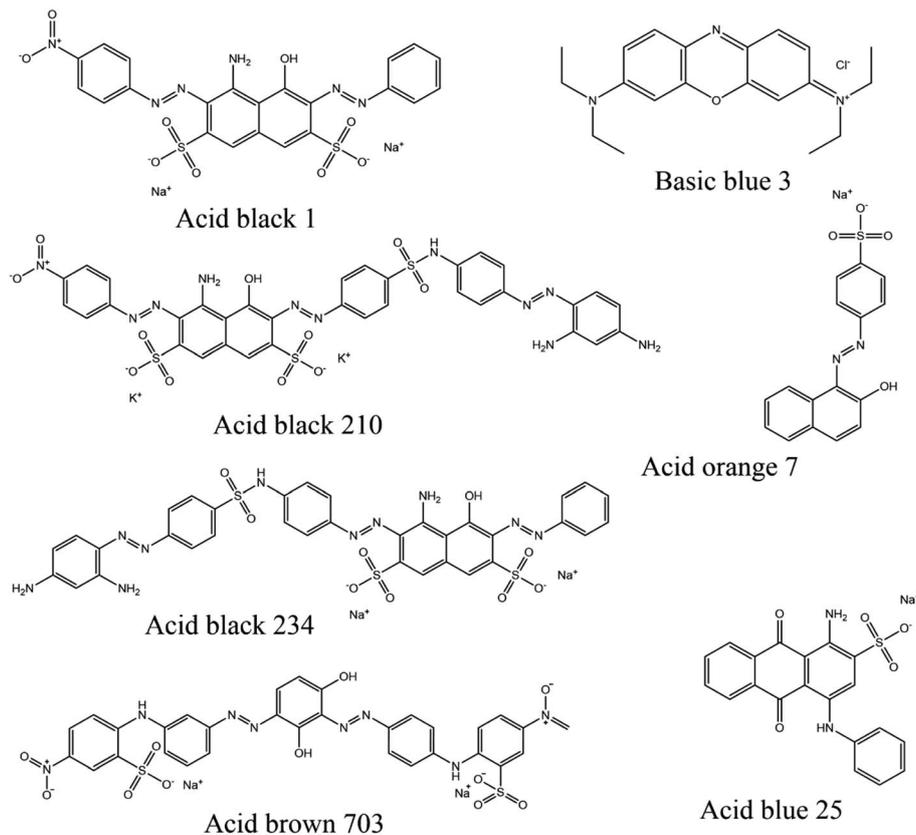
Fig. 1 Structures of the dyes: acid black 1 (Mw. 616.49 g mol^{-1} λ_{max}. 618 nm), acid black 210 (Mw. 938.02 g mol^{-1} λ_{max}. 604 nm), acid brown 703 (Mw. 794.63 g mol^{-1} λ_{max}. 471 nm), acid black 234 (Mw. 860.8 g mol^{-1} λ_{max}. 642 nm), basic blue 3 (Mw. 359.89 g mol^{-1} λ_{max}. 654 nm), acid orange 7 (Mw. 350.32 g mol^{-1} λ_{max}. 485 nm), acid blue 25 (Mw. 416.38 g mol^{-1} λ_{max}. 600 nm). Mw = molecular weight.

the % removal of the template dye from different water samples were more than 90%. These MIPs can be employed as SPE-MIP cartridges for the quantification of these dyes for their reuse in different applications.

2. Materials and methods

2.1. Chemicals and materials

Ethylene glycol, methacrylic acid, AIBN, methanol, acid black 1, acid orange 7, acid blue 25, and basic blue-3 were purchased from Sigma Aldrich. Acid black 210, acid black-234, and brown 703 were donated by the Sofeene Enterprises (a branch of the Singapore company located in Pakistan). The company also provided the chemical structure, molecular weight, and wavelength of maximum absorption of these dyes, which are given in Fig. 1. Acetone and water: Mallinckrodt Baker (Phillipsburg, NJ, USA). The reagents were used as received from the respective companies. The tubing (glass-lined stainless-steel) was purchased from Grace (Deerfield, IL, USA), which was 15 cm long with 1 mm id, 1/8 inch od. Silica capillaries with 50 μm internal diameter (ID) and 365 μm outer diameter (OD) were received from Grace (Deerfield, IL, USA). Methanol (high grade), acetonitrile, and acetone along with water were purchased from Mallinckrodt Baker (Phillipsburg, NJ, USA).

2.2. The synthesis of acid black 1, acid black 210 and brown 703 imprinted polymers

MIP-1, MIP-2, and MIP-3 with the specific cavities for the targeted template dyes, namely acid black 1, acid black 210 and acid brown 703, respectively, were synthesized using the radical polymerization protocol. The reaction mixture consisted of ethylene glycol as the cross-linker, methacrylic acid as the monomer, azo-bis-isobutyronitryl (AIBN) as the initiator, methanol as the porogenic solvent media along with the targeted template molecule (dye). The mixing ratios among the reacting ingredients were kept as 1 (template):10 (functional monomer):44 (cross-linker). The exact amounts of all the reacting ingredients for the synthesis of all three MIPs have been summarized in Table 1. The reaction mixture was polymerized in a water bath at 60 °C for 24 h. A two-step washing strategy was used. In step 1, the MIPs were washed with methanol three times to remove the unreacted/ unbonded template, monomers, crosslinker, and AIBN. In step 2, the MIPs were washed with 1 : 9 (V/V%) acetic acid/ methanol thrice for the removal of bonded template molecules from the MIP network. As a result of the second washing step, the templates left their imprint cavities in the MIPs. The washed MIPs were dried at room temperature and ground off.

Table 1 Amount of the reagents used in the synthesis of the MIPs (acid black 1, acid black 210 and acid brown 703)

Reagents	AB-1	AB-210	AB-703
Template/dye	0.06 g	0.09 g	0.08 g
Functional monomer (MAA)	90 µL	90 µL	90 µL
Cross linker (EG)	250 µL	250 µL	250 µL
Initiator (AIBN)	0.03 g	0.03 g	0.03 g
Porogen (methanol)	62 ml	94 ml	80 ml

2.3. Kinetic studies

The highest output of the newly synthesized MIPs for the removal of their respective dyes from solution was determined by optimizing various parameters such as pH, contact time, dosage, and concentration.

The adsorption mechanisms of the prepared MIPs were studied by applying the pseudo-first-order, pseudo-second-order and intra-particle diffusion models. The procedure of the experiment involved the addition of 0.020 g of the synthesized polymers (MIPs) to a 10 ml (100 ppm) solution of the dye being taken in 10 different tubes at constant pH. The samples in various tubes were subjected to different shaking times, starting from 5 min up to 50 min with a time interval of 5 minutes each. The adsorption at time t (Q_t in mg g^{-1}) was calculated using the following formula:

$$Q_t = (C_o - C_t) \, V/M \tag{1}$$

where C_o and C_t (mg L^{-1}) are the liquid-phase concentrations of the dye initially and at any time t, respectively. V is the volume of the solution (l) and M is the mass of dry adsorbent used (g).

2.4. Batch equilibrium studies

Adsorption isotherms were accomplished in a set of 43 Erlenmeyer flasks (250 ml) where solutions of dye (100 ml) with different initial concentrations (20–175 mg L^{-1}) were taken in different flasks. Here, 0.03 g, 0.04 g and 0.02 g of polymeric materials MIP 1, MIP 2 and MIP 3 were added to the dye solutions taken in different tubes. The tubes containing MIP 1, MIP 2 and MIP 3 were kept in an isothermal shaker for 30, 25 and 40 minutes, respectively to reach the equilibrium of the solid-solution mixture. The pH of the solutions was adjusted to 3, 2 and 5 by adding either a few drops of diluted hydrochloric acid (HCl) or sodium hydroxide (NaOH). The final concentrations of the dyes in their respective solutions were analysed. Finally, the amount of adsorption Q_e (mg g^{-1}) at equilibrium was calculated using the equation

$$Q_e = (C_o - C_e) \, V/M \tag{2}$$

where C_o and C_e (mg L^{-1}) are the liquid-phase concentrations of the dye at the initial stage and equilibrium, respectively. V is the volume of the solution (l), and M is the used mass in (g) of dry adsorbent.

2.5. The set-up of the liquid chromatography system

A homemade HPLC system was designed as reported in by our research group.[45,46] It took a capillary window detector (UV-2075), a Shimadzu pump (10AD), an injector with a 50 nL injection loop (C14W.05), and a membrane degasser (DGU-14A) for its construction. The acquisition and processing of the chromatographic data were carried out on software (Multichrow 2000 from Yullin Technology, South Korea) installed on a computer connected to the detector.

2.6. The art of column assembly and packing

Column parts were connected in accordance with the experience being practised in our laboratory.[48,49] Here, 150 mm long stainless-steel columns with 1 mm internal diameter were packed with the MIP-structured stationary phases. The flow sheet diagram showing the setup of the column packing (particle packing machine) has been previously reported by our research group in the supplemental materials.[49] A slurry of the MIP particles was prepared in methanol. The slurry was fed into the column using the packing machine provided with a tapering reservoir. The packing process was assisted by vibrations of the column and reservoir.

The capacity of the reservoir was 12 mL while the amount of the stationary phase (MIP particles) was 750 mg. Three different columns of the same dimensions were packed with three different MIP materials (MIP-1, MIP-2, and MIP-3). The packed column was then connected to the HPLC pump (Shimadzu Company) on one side while the second side of the column was connected to the UV detector. All three columns were finally tested one by one for the separation of five different dyes with closely related chemical structures.

3. Results and discussion

3.1. Characterization of unwashed and washed MIPs

3.1.1. Fourier transform infra-red spectroscopy. All the samples of the MIPs were washed using the step-1 washing protocol. The samples of MIPs were analysed before and after the second washing step in the FTIR range of 4000–500 cm^{-1}.[50] Similarly, the powdered dyes (acid black 1, acid black 210, and acid brown 703) were characterized by their FTIR spectra, which are given in the ESI.† Most of the corresponding peaks of MIP-1, MIP-2 and MIP-3 are related to each other. The similar characteristic peaks in all the MIP samples are mainly due to the same constituents of the MIPs. The only differences between the three MIPs are their templates. The peaks in the ranges of 3400–3300 cm^{-1} and 1350–1342 cm^{-1} are due to N–H and SO$_3$H of the imprinted molecules, respectively,[50–52] as given in Fig. 2. Peaks at 1700, 1701 and 1702 cm^{-1} of MIP-1, MIP-2 and MIP-3 are due to the stretching vibration of C=O of the functional monomer (MAA).[52–55] The peaks observed at 1081, 1084, and 1083 in the IR spectra of MIPs show the presence of the C–OH group in the cross-linker (EG).[50,51] The presence of small peaks in the range of 600–900 cm^{-1} in the IR spectra of template-bound MIPs indicates the hydrogen bonding interactions between the template and MIPs given in Fig. 2(A, B and C). The
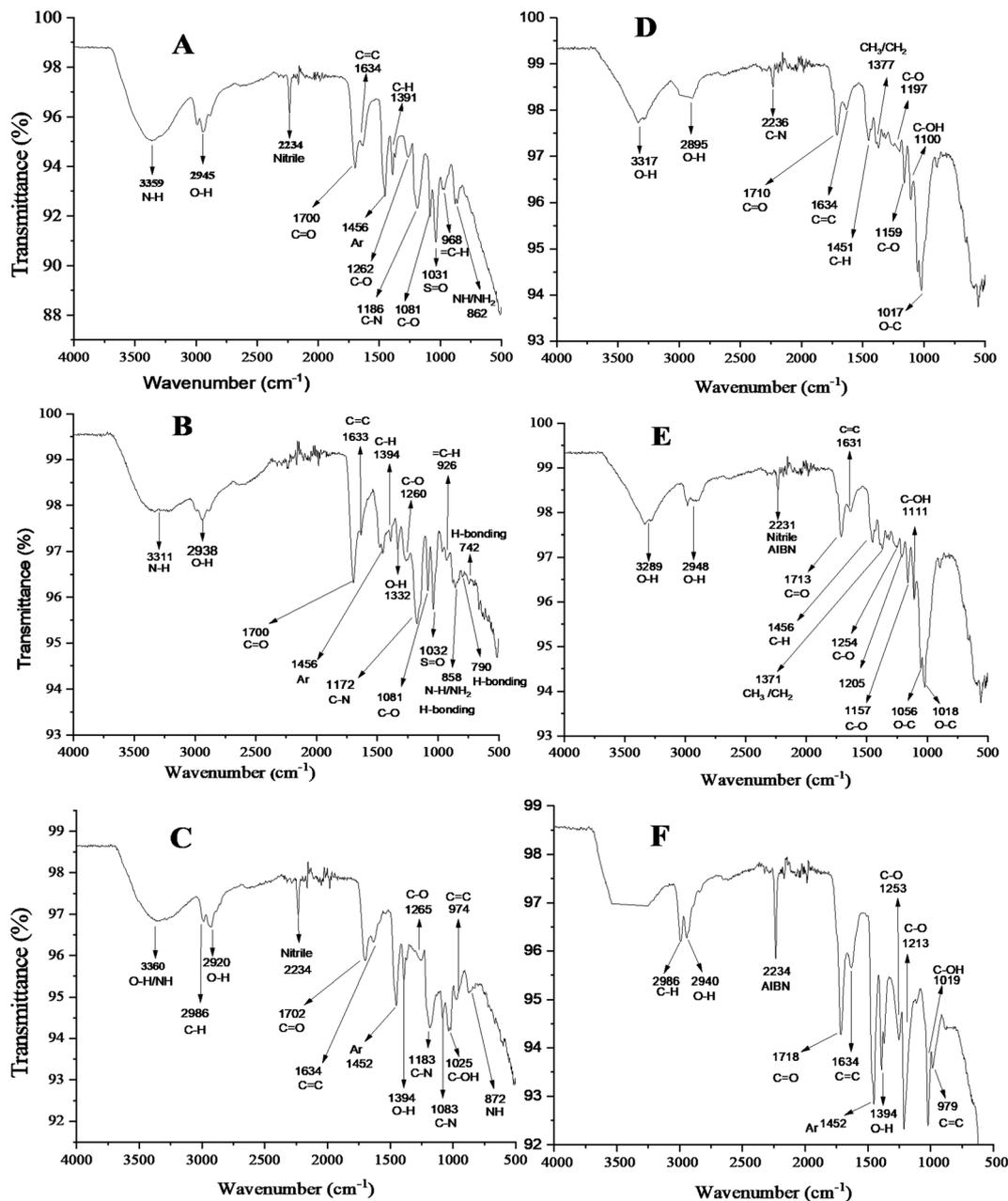
Fig. 2 FTIR spectra of the template-bound MIP-1 (A), MIP-2 (B) and MIP-3 (C) and template-removed MIP-1 (D), MIP-2 (E) and MIP-3 (F).

very low intensities of the peaks in the range of 600–900 cm^{-1} are due to the very small ratio of the template molecule in comparison to those of the other reacting species (template : monomer : cross-linker; 1 : 10 : 44). The disappearance of those peaks in the IR spectra of step-2 washed (template removed) polymers given in Fig. 2(D, E and F) are due to the elution of the template from their respective MIPs.[56] The FTIR spectra of the dyes contain peaks representing their characteristic functional groups.[57,58] The relevant information of all the peaks along with their functional groups are given in the FTIR images. The comparison of the FTIR spectra of the dyes (template) to those of their corresponding MIPs (template

encapsulated) showed a marked difference that suggests the formation of the MIP synthesis. The disappearance of the peaks at 3425 cm^{-1}, 2089 cm^{-1}, 1225 cm^{-1}, 758 cm^{-1}, 690 cm^{-1}, and 600 cm^{-1} in the spectrum of the template-bound MIP for acid black 1 is due to the binding of the template inside the MIP cavity. Similarly, the presence of peaks at 1637 cm^{-1}, 1587 cm^{-1}, 1534 cm^{-1}, 1485 cm^{-1}, 1331 cm^{-1}, 1141 cm^{-1}, 643 cm^{-1}, 567 cm^{-1}, 596 cm^{-1}, and 530 cm^{-1} in the spectrum of the dye and the disappearance of those peaks in the template-bound spectrum of the MIP is an indication of the template binding within the MIP cavities. The presence of the broad peak at 3360 cm^{-1} instead of comparatively sharp peaks at

(3610 cm^{-1}, 3329 cm^{-1}, and 3311 cm^{-1}) and the presence of the broad peak at 2986 cm^{-1} instead of the sharp peak at 3030 cm^{-1} in the template-bound MIP of acid brown 703 in comparison to the spectrum of the dye powder indicate template binding inside the MIP cavities. The disappearance of the peak at 2481 cm^{-1}, 810 cm^{-1}, 790 cm^{-1}, 736 cm^{-1}, and 659 cm^{-1} in the spectrum of the template-bound MIP indicates template binding inside the MIP structure.

3.1.2. **Scanning electron microscopy.** The morphological and architectural appearance of the polymers were visualized in the form of SEM imaging summarized in Fig. 3. All the SEM snapshots indicated the porous natures of the MIPs. The causative agent for the generation of pores is methanol, which has been used as a solvent in the polymerization process. The expanded view of the SEM image of a single MIP-3 particle after the removal of the template molecule shows the cavitation. SEM imaging is a useful characterization technique for the confirmation of particle size distribution. The particle size distribution for each of the MIPs was in the range of 1–3 μm (determined using a Master sizer) which is in strong agreement with the particle size shown in the SEM images for the individual MIP sample.

3.1.3. **The effects of pH, time, dosage, and concentration on adsorption.** The effect of pH on dye adsorption onto the newly synthesized MIPs was investigated at different pH values ranging from 1 to 7. Maximum adsorption of the dyes AB-1, AB-210, and AB-703 were found to occur at pH values of 3, 2, and 5,

respectively, as shown in Fig. 4A. Generally, the adsorption capabilities of the acidic dyes are higher at lower pH since the lower pH renders the solution interface more positively charged, which ultimately appears on the surface of the adsorbent.[59–62] Acid dyes interact better under acidic conditions since the sulfonate group will interact with any positive charge on the surface of the MIP.

There are lone pairs of electrons on some of the functional groups present in the skeleton of the MIPs. At lower pH, a greater number of hydrogen ions accumulates on the surface of the MIPs owing to the attractive forces between the hydrogen ions and lone pairs of electrons. As a result, the surface of the MIP adopts a positively charged layer at its surface. Since the dyes are acidic, they are negatively charged at lower pH values. The negatively charged dyes have higher electrostatic interactions with the positively charged MIPs. This is why the MIPs can hold higher concentrations of the dyes at lower pH values due to the strong electrostatic interactions existing between the negatively charged adsorbate and positively charged adsorbent. Nevertheless, at extremely lower pH, the negative charge on some of the acidic dyes may participate in electrostatic interactions with the hydrogen ions. Depending upon the magnitude of the negative charge on the individual dye, the electrostatic interactions are different. Each acidic dye has a different magnitude of negative charge at its surface at the same pH. This leads to different optimum pH values for the different acidic dyes.
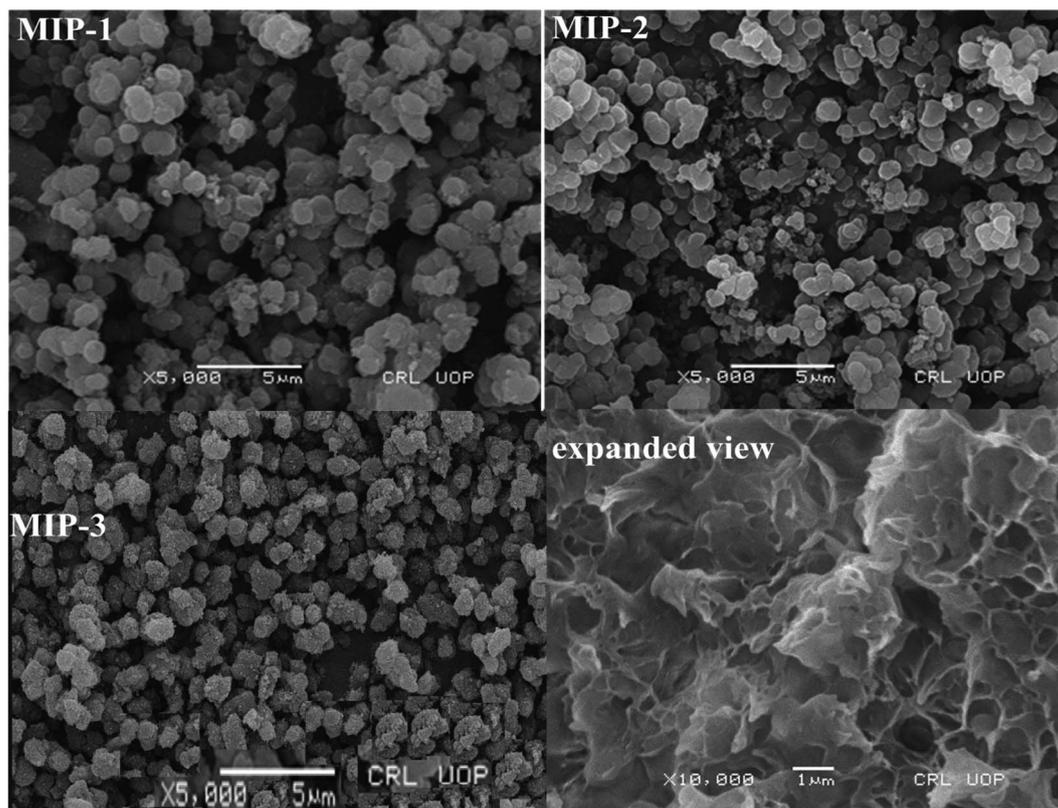

Fig. 3 SEM micrographs of MIP-1, MIP-2, and MIP-3. Expanded view of a single MIP particle of MIP-3 after the removal of the template molecule.
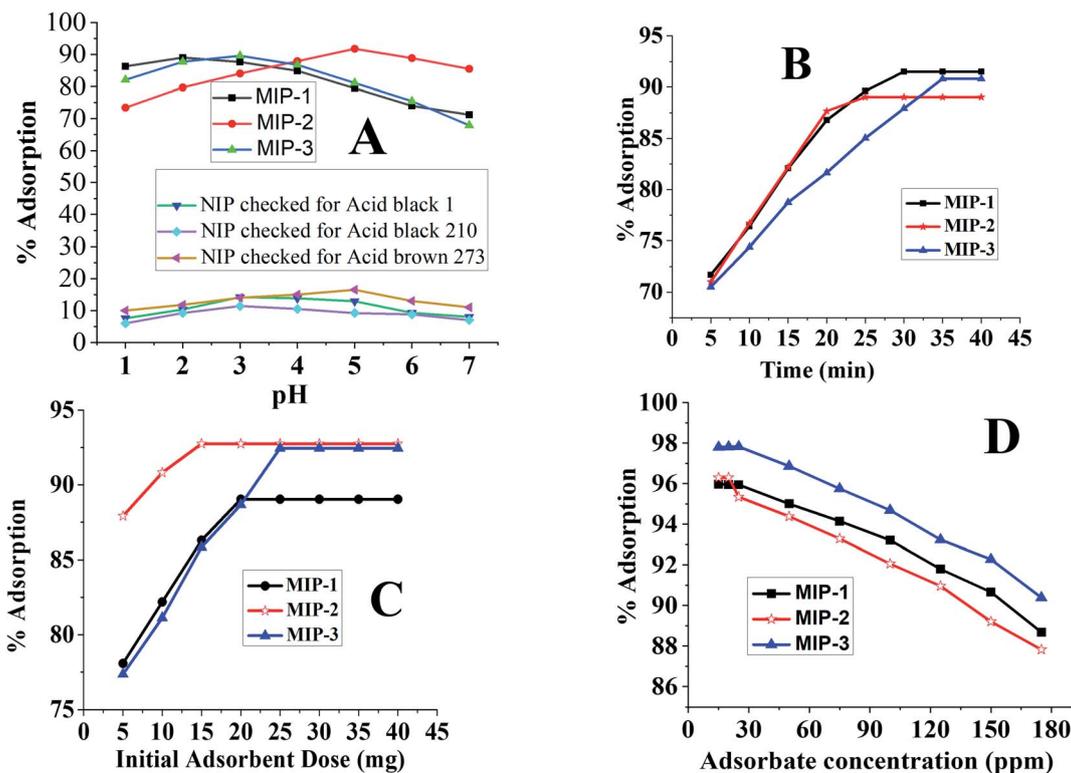
Fig. 4 Optimization curves of pH (A), time (B), adsorbent dosage (C) and initial adsorbate concentration (D) for MIP-1, MIP-2 and MIP-3. The pH optimization curve for the NIP is given in (A).

The pH values of the solutions were adjusted by the dropwise addition of diluted hydrochloric acid or sodium hydroxide. The trends of the pH effect on the adsorption of the dyes (acid black-1, acid black-210, and acid brown-703) on the NIPs were like those obtained on the adsorption of the dyes onto their respective MIPs. The optimized pH for the maximum % adsorption of the dye's acid black-1, acid black-210, and acid brown-703 onto the NIP were 3, 3, and 5, respectively.

The optimum equilibrium times were found to be 30 min, 25 min, and 35 min for the dyes AB-1, AB-210, and AB-703, respectively, which are summarized in Fig. 4B. Beyond the optimized times, the adsorption remained constant since the MIP surfaces were saturated with their dyes.[50]

The effects of the MIP amount on the adsorption of their corresponding dyes have been analysed for all three MIP-based adsorbents through batch analysis. The optimized amount of the MIP-1, MIP-2, and MIP-3 were found to be 20 mg, 15 mg, and 25 mg, respectively.

To check the dosage effect, different amounts of the individual MIPs were taken in the range of 0.005–0.08 g. The optimized amounts of the MIPs were found to be 20 mg (AB-1), 15 mg (AB-210) and 25 mg (AB-703) see Fig. 4C. An increase in the extent of adsorption by increasing the amount of MIP indicated the sample loading capacity of the individual MIP. Each MIP has its own sample loading capacity. The % adsorption remained constant beyond a certain point/loading capacity of the MIP[50,59,62] since the surface saturation of the MIPs was

achieved at the point of the sample loading capacity of the sorbent.

The initial adsorbate concentration effect on the % adsorption of all three MIP templates was investigated. The initial concentration ranges of MIP-1, MIP-2, and MIP-3 were 5–50 ppm, 20–160 ppm, and 25–200 ppm, respectively. In Fig. 4D, initially, the small concentration had no effect on the % adsorption but the % adsorption decreased with higher adsorbate concentration. This is because of the increment in the adsorbate/adsorbent ratio and saturation of the adsorbent surface.[50,62] To confirm the optimized ppm for the respective MIPs, the concentrations of the dyes below 5, 20 and 25 ppm were also investigated and were found to be almost constant.

3.1.4. Kinetics study. The plots obtained because of the kinetics study for the MIPs and NIP are given in Fig. 5. The adsorption mechanism is determined by applying the pseudo (first and second) order and Morris–Weber kinetic models.[54,63] The pseudo-first-order equation reported by Lagergren and Svenska is as follows:[63,64]

$$\log(q_e - q_t) = \log q_e - k_1 t/2.303$$

where q_e and q_t indicate the amount of dye (mg g^{-1}) adsorbed at equilibrium and at time t (min). k_1 refers to the rate constant of adsorption,[64] which is min^{-1}. The numerical values of k_1 were calculated from the plots drawn for different concentrations of dye between $\log(q_e - q_t)$ against t, which are 0.11722, 0.167, and 0.074 for the MIP 1, MIP 2 and MIP 3, respectively.[63] Similarly,
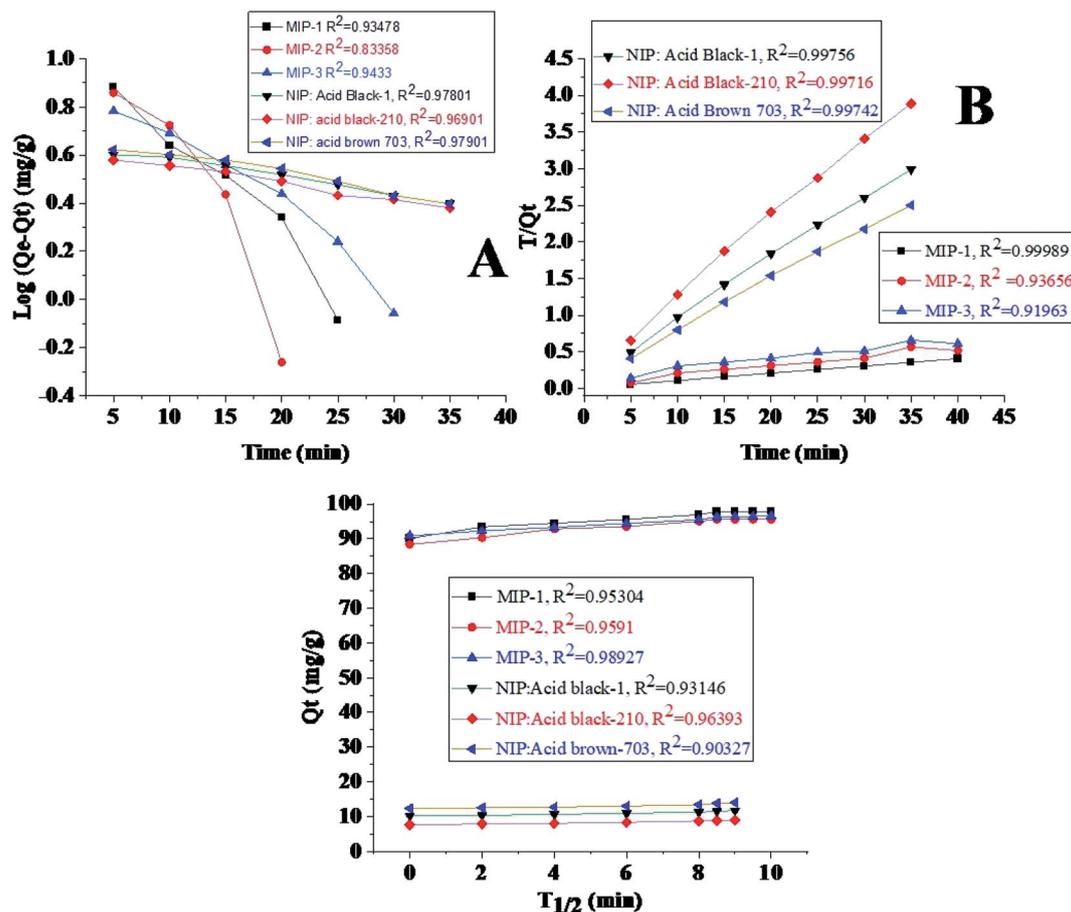
Fig. 5 The pseudo-1st-order kinetic (A), pseudo-2nd-order kinetic (B), and Morris–Weber models (C) for the MIPs (1, 2, and 3) and NIPs.

the pseudo-second-order kinetic equation was also applied to analyse the sorption data[63] being expressed as

$$t/q_t = t/q_e + 1/k_2\,q_e^2$$

where k_2 is the rate constant (min. g mg^{-1}) of the pseudo-second-order kinetic equation. If the second-order model is applicable, the plots of t/qt against t should be a linear relationship.[65] The K_2 and q_e can be calculated from the intercept and slope of the plots, which are 0.01069, 0.0106, and 0.0101 for MIP-1, MIP-2 and MIP-3, respectively. A linear plot of t/q_t versus t proves the applicability of the second-order kinetic model and the second-order nature of the adsorption process for the dye. A comparison of the correlation coefficients of both kinetic orders indicated that the R_2 values of the pseudo-second-order model are greater than those of the pseudo-first-order model as shown in Fig. 5. It revealed that the adsorption of AB-1, AB-210 and AB-703 on MIP-1, MIP-2, and MIP-3 respectively, best follow the second-order model.[64,65]

3.1.5. Intra-particle diffusion model. Adsorption involves not only the accumulation of dye molecules on the surface but also the possibility of intra-particle diffusion.[66,67] Pore, film diffusion, and intra-particle transfer are the three steps that affect the adsorption mechanism.[64] The intra-particle diffusion is more likely a batch experiment analysis.[68,69] The Weber and

Morris (intra-particle diffusion) model was used to investigate the mechanism of adsorption, as shown below.

$$Q_t = K_d t_{1/2} + I$$

K_d is the intra-particle diffusion rate constant, and I is the intercept that reflects the boundary layer effect. Values of different constants were computed from the plot of Q_t vs. $t_{1/2}$, which are summarized in Fig. 5. The plots in Fig. 5(G, H and I) indicated time limits where the rate-controlling steps are in strong agreement with the intra-particle diffusion within those time limits. The plot line for MIP-1 and MIP-2 passed through the origin for up to 10 min each while that of MIP-3 reached up to 15 min. It means that up to that time, the rate-controlling steps follow the intra-particle diffusion, while above that time additional surface phenomena are involved.

3.1.6. Adsorption studies. The adsorption isotherms for the MIPs and NIP are summarized in Fig. 6. The adsorbate–adsorbent interactions are well interpreted by the execution of adsorption studies. The adsorption studies have been carried out in detail to determine the distribution of adsorbate both in solution and adsorbent at equilibrium. The two well-known isotherm models (Freundlich and Langmuir) were applied to the newly fabricated MIPs for the determination of the adsorption capacity of all the MIPs (MIP-1, MIP-2 and MIP-3).[70]
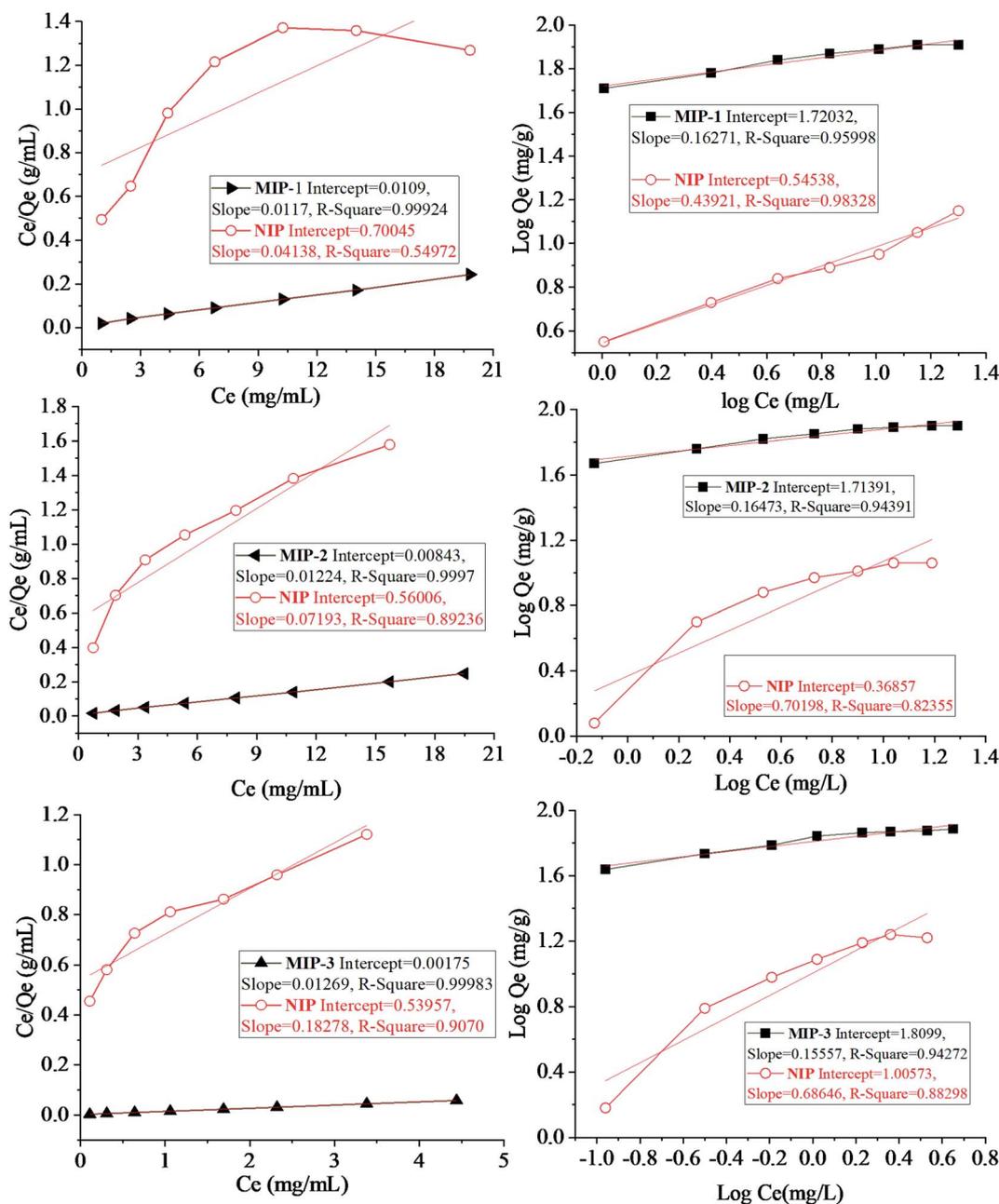
Fig. 6 Left: Langmuir adsorption isotherms and right: Freundlich adsorption isotherms for MIP-1, MIP-2, and MIP-3. The corresponding isotherm plots for the NIPs are also given.

The Langmuir model is applicable to the monolayer adsorption surfaces having a definite number of binding sites as well as uniformity of energy involved in the polymer–template interactions.[71] A single adsorbate molecule can occupy a single site on the surface[13,15,71–73] which results in a uniform adsorbent surface.[74] The mathematical form of the model is reported in ref. 75.

$$C_e/Q_e = 1/KLQ_o + C_e/Q_o$$

C_e: equilibrium concentration of the dye in solution (mg L^{-1}), Q_e: the amount of the adsorbed dye at equilibrium (mg g^{-1}) while KL: Langmuir constant.

The Langmuir equation has been applied to the data taken from the plots being plotted between C_e/Q_e vs. C_e for the MIPs under study. The values of KL and Q_o were calculated from the plots using the values of the intercept and slope. The values of KL for MIP-1, MIP-2 and MIP-3 were computed to be 24.213, 24.875, and 36.63, respectively while the values of Q_o were calculated to be 228.424, 188.67, and 97.25, respectively. The important features of the Langmuir isotherm may be shown in the form of an equilibrium parameter having no dimensions, called the separation factor (RL).

$$RL = 1/(1 + KL\ C_o)$$

C_o = initial concentration KL = constant related to the adsorption energy. Through the computation of the "RL" value, it was confirmed that adsorption was favourable for the MIP under investigation since the "RL" values were smaller than 1 and greater than 0.[75]

The surfaces exhibiting multilayer adsorption, usually the heterogeneous surfaces, are more suitably studied by the application of the Freundlich model and the related adsorption isotherm. Energies of the binding sites will be non-uniform.[76,77] According to ref. 78 the linear form of the Freundlich equation can be expressed as

$$\log Q\mathrm{e} = \log K_f + 1/n \log C$$

K_f is related to the adsorption capacity of the adsorbent (mg g^{-1}), n is the adsorption intensity, while Q_e is the amount of dye adsorbed on the surface of one gram of MIP at equilibrium. $1/n$ expresses the heterogeneity parameter. The values of 'n' and 'K_f' can be calculated by plotting the data between Q_e and C_e. When the value of $1/n$ is smaller than 1 and $n = 1$–10, then the surface will be heterogeneous and adsorption will be linear and feasible.[71,79] The applicability of these isotherms to the newly synthesized MIPs can be determined by plotting the curves from the experimental data given in Fig. 6 The R^2 values of the Langmuir models for all the MIPs were higher than those of the Freundlich model. The best-fitting model applicable to the newly reported MIPs was the Langmuir adsorption model, which was confirmed by the comparison of the correlation coefficients of both models.

3.1.7. Selective nature of the MIPs. The affinities of the newly synthesized MIPs for their respective template dyes were investigated by comparing their affinities to those of the NIP (polymer prepared without a template) for the same template molecule. While the selectivity of those MIPs was confirmed by testing the adsorption capabilities for their respective templates in the presence of other dyes that are similar in structure to their template molecules in terms of their chromophores such as acid black 234 and acid orange 7. At the same time, other acid dyes that are dissimilar in structure to the dyes of the synthesized MIPs in terms of the basic skeleton such as acid blue 25 and a basic dye (basic blue 3) were also present in the solution. The adsorption capacities of various dyes on MIPs and NIPs and the experimental results achieved because of the adsorption of acid black 1, acid black 210, and acid brown 703 onto their respective MIPs and NIPs are given in Table 2. For comparison purposes, the adsorption results of the acid black 234 and basic blue 3 onto each of the MIPs and NIPs are also presented in Table 2. The adsorption capacities of AB-1, AB-210 and AB-703 on their respective MIPs are much higher than those of the acid black 234, acid orange 7, acid blue 25, and basic blue 3, on each of the MIPs. The adsorption capacities of acid black 234, acid orange 7, and acid blue 25 are higher than those of the basic blue 3 on each of the MIPs, which might be due to the structural similarities of these acidic dyes to those of the AB-1, AB-210 and AB-703 in contrast to the structure of BB-3. The adsorption capacities of the AB-1, AB-210 and AB-703 on the NIPs are close to each other but lower than those on MIPs,

Table 2 Comparison of the selectivity adsorption studies of MIP-1, MIP-2 and MIP-3 with those of the NIPs

Templates/dyes	Percent adsorption (%)			
	MIP-1	MIP-2	MIP-3	NIP[a]
Acid black 1	96.5	25.2	27.5	33.4
Acid black 210	32.7	95.3	26.1	31.9
Acid brown 703	27.7	21.0	96.9	34.6
Acid black 234	27	34.2	26.8	23
Acid orange 7	20	25	28	21
Acid blue 25	22	19	16	17
Basic blue 3	9.2	11	10.1	7.4

[a] The corresponding NIP of all the MIPs is the same since they have the same formulation, except for the template.

indicating the better selective adsorption capabilities of the MIPs for their respective template molecules. The selection of various dyes with different basic skeletons is critical for the selectivity study of the MIPs.

3.1.8. Application of the MIPs in real samples. The efficiencies of MIPs for the extraction of acid black 1, acid black 210, acid brown 703, acid black 234, acid orange 7, acid blue 25, and basic blue 3 were evaluated by applying the washed MIP1, MIP2, and MIP3 to the environmental samples including distilled, tap, and river water samples. The samples were spiked with known quantities of the dyes (100 mg L^{-1}). The process was carried out under optimized conditions. The selective and efficient removal of the dyes from different water samples was determined, which is summarized in the Table 3. The successful selective removal of the specific dyes by their corresponding MIPs from water samples is due to the memory effect of the imprinting molecule.

3.1.9. Liquid chromatography method for the characterization of MIPs. The real-time separation of different dyes using a column packed with the individual MIPs was carried out on a home-assembled HPLC system. The MIPs were crushed into powder and packed in a 150 mm long stainless-steel column with an internal diameter of 1 mm using an Alltech slurry packer. The particle size distribution using the master sizer showed that the particle sizes were in the range of 1–3 μm for the three MIPs. All three MIP-based stationary phases were packed in different columns of the same dimensions. Three different columns were packed with MIP-1, MIP-2, and MIP-3. The packing protocol reported in ref. 48 and 49 was used for packing the columns. The columns were installed in a home-made HPLC system constructed in accordance with the steps used in ref. 49 All three columns were evaluated for the separation of a mixture of dyes containing at least one dye for which the cavities were already been imprinted in the polymer stationary phase. The chromatograms A, B, and C in Fig. 7 were obtained on the column packed with MIP-3, MIP-2, and MIP-1, respectively. The last eluting peak in each chromatogram is the peak of the template dye for which the corresponding cavities were imprinted in the polymer stationary phase. The cluster of three peaks located in the middle of the chromatograms corresponds to the dyes that are similar in structure to the

Table 3 Efficiency of MIP-1, MIP-2, and MIP-3 in terms of % recovery of the dyes

Sample	MIPs	% Recovery of the dyes with % SD						
		AB-1[a]	AB-210[a]	AB-703[a]	AB-234[a]	AO-7[a]	AB-25[a]	BB-3[a]
Distilled water	MIP-1	96 ± 3	33 ± 3	28 ± 3	28 ± 4	38 ± 3	35 ± 3	09 ± 3
	MIP-2	27 ± 2	95 ± 3	22 ± 2	34 ± 3	24 ± 3	29 ± 1	11 ± 3
	MIP-3	29 ± 3	27 ± 3	97 ± 2	32 ± 4	27 ± 3	28 ± 2	8 ± 4
Tap water	MIP-1	95 ± 3	34 ± 2	36 ± 3	30 ± 3	36 ± 2	36 ± 3	9 ± 2
	MIP-2	28 ± 3	93 ± 4	23 ± 3	34 ± 3	35 ± 3	35 ± 3	10 ± 4
	MIP-3	26 ± 3	28 ± 3	95 ± 2	30 ± 3	25 ± 2	25 ± 3	8 ± 3
River water	MIP-1	93 ± 2	32 ± 2	33 ± 2	28 ± 3	35 ± 4	33 ± 2	9 ± 3
	MIP-2	27 ± 3	91 ± 3	25 ± 4	34 ± 3	31 ± 2	33 ± 3	11 ± 4
	MIP-3	33 ± 2	29 ± 4	94 ± 2	28 ± 3	30 ± 3	30 ± 2	9 ± 4

[a] Volume of each dye added to each sample was 20 mL, while the spiking amount of each dye to each sample was 100 mg L^{-1}. The template dyes for MIP-1, MIP-2, and MIP-3 are AB-1, AB-210, and AB-703, respectively.

template dye. The comparatively weak resolution of the cluster of three peaks suggested similarities in structure. The excellent resolution achieved for the template dye is in strong agreement with the excellent selectivity of the MIPs for their respective dye molecules. The longest retention time of the template molecule in the corresponding MIP-packed column is due to the long time spent by the molecule in the cavities being imprinted in the stationary phase for that dye. Due to the structural similarities, three other dyes have close retention times with poor resolution. The resolution for other dyes is poor in comparison to that achieved for the target dye for each of the MIP. While the first eluting peak in chromatograms (B and C) corresponds to the basic blue-3 dye. The earlier elution of the basic dye indicated that the acidic template-imprinted MIP stationary phases have little affinity for the basic dyes.
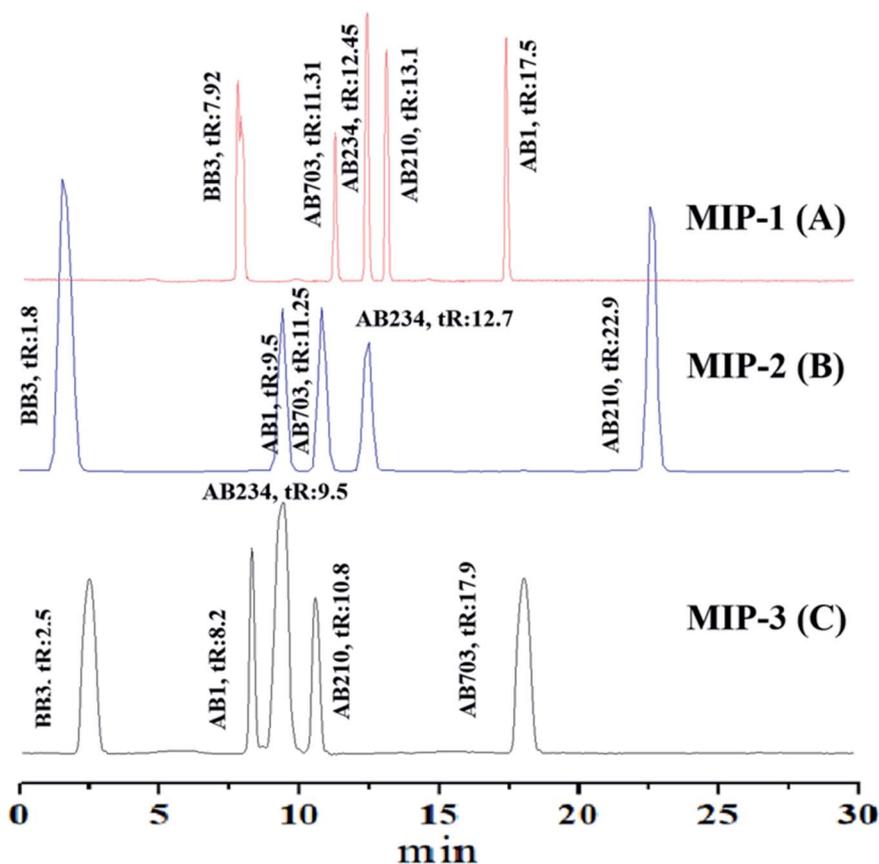

Fig. 7 Chromatograms obtained using the columns packed with MIP-1 (A), MIP-2 (B), and MIP-3 (C), and column dimensions: 150 mm long, 1 mm ID. Mobile phase: methanol/water 80/20 (*v/v*%), 0.1% trifluoroacetic acid. The detection wavelength was 624 nm. Eluent flow rate: 40 μL min^{-1}. Each peak has been labelled with the name of its corresponding dye and retention time (t_R) in min.

Table 4 The parameters calculated from the most suitable kinetic models and isotherms for MIP-1, MIP-2 and MIP-3

	parameters	MIP-1	MIP-2	MIP-3
Kinetic	K1	0.1172	0.1670	0.0741
	K2	0.0106	0.0106	0.0101
Adsorption	Q_o	228.4242	188.6765	97.2525
	KL	24.2131	24.8755	36.6315
	RL	0.0004	0.0004	0.0002

In the current study, the elution time of the dyes is a little longer. The long elution time of the dyes in comparison to those of the dyes reported on the C18 column is due to the increased interaction of the dyes with their respective MIPs. The short and long retention times of dyes confirmed the formation of cavities in their MIPs but the resolution between two adjacent pairs of dyes is better than those reported on C18 columns.[80,81] The presence of two sulfonate groups on the acid dyes seems to have no significant effect on the separation of such dyes.

The construction of a homemade liquid chromatographic system, the assembly and packing of the column with MIP-based stationary phases, and availing the liquid chromatography system for the evaluation of selectivity studies of the MIPs are quite interesting. The LC being developed in the current study is a very good characterization tool for the selectivity investigations of different MIPs (Table 4).

4. Conclusion

MIPs for acid black 1 (MIP-1), acid black 210 (MIP-2), and acid brown 703 (MIP-3) dyes were synthesized, characterized, packed in stainless steel columns, and tested for the separation of a mixture of dyes both under batch analysis and in a liquid chromatography system. The main objective of the current study was the synthesis of selective adsorbent materials (MIPs) and their application in the removal of the dyes from different water samples. Each of the MIP-packed columns resulted in the long retention time of the dye, which is complementary in structure to the cavities imprinted in the MIP stationary phase revealing the highly selective nature of the MIPs for their corresponding template. The % RSD, in view of the separation efficiency and retention times, were found to be less than 4%. The batch adsorption studies of the MIPs indicated that the pH of the solution was the critical determinant of the adsorption capacities of the MIPs. The maximum adsorption was found to occur at the pH values of 2 (MIP-1), 3 (MIP-2), and 5 (MIP-3), having the optimum equilibrium times of 30 min, 25 min, and 35 min respectively. The optimum doses of the MIPs were 20 mg (MIP-1), 15 mg (MIP-2), and 25 mg (MIP-3). The highest % adsorption computed at the optimum values of the adsorption parameters were 99.3%, 99.1%, and 98% for the MIP-1, MIP-2, and MIP-3, respectively. SEM photographs confirmed the cavities left behind by the elution of the template in the MIPs, and the FTIR spectra showed that the peaks for the functional groups corresponding to the monomer reagents were present. Adsorption of the templates onto the MIPs followed the 2nd order kinetic model and the data were best fitted in the Langmuir isotherm model.

Conflicts of interest

There are no conflicts to declare.

References

1 O. A. Kareem, *Res. J. Text. Appar.*, 2012, **16**, 79–92.
2 M. S. Frey, *J. Chem. Educ.*, 1981, **58**, 301–305.
3 V. Sharma, H. T. McKone and P. G. Markow, *J. Chem. Educ.*, 2011, **88**, 24–28.
4 A. Bafana, S. S. Devi and T. Chakrabarti, *Environ. Rev.*, 2011, **19**, 350–370.
5 V. K. Gupta and Suhas, *J. Environ. Manage.*, 2009, **90**, 2313–2342.
6 B. Okutucu, A. Akkaya and N. K. Pazarlioglu, *Prep. Biochem. Biotechnol.*, 2010, **40**, 366–376.
7 P. K. Malik, *Dyes Pigm.*, 2003, **56**, 239–249.
8 F. R. Abe, A. L. Machado, A. M. V. M. Soares, D. P. de-Oliveira and J. L. T. Pestana, *Chemosphere*, 2019, **236**, 124390.
9 E. Forgacs, T. Cserhati and G. Oros, *Environ. Int.*, 2004, **30**, 953–971.
10 M. V. Foguel, N. T. B. Pedro, A. Wong, S. Khan, M. V. B. Zanoni and M. P. T. Sotomayor, *Talanta*, 2017, **170**, 244–251.
11 F. I. Vacchi, A. F. Albuquerque, J. A. Vendemiatti, D. A. Morales, A. B. Ormond, H. S. Freeman, G. J. Zocolo, M. V. B. Zanoni and G. Umbuzeiro, *Sci. Total Environ.*, 2013, **442**, 302–309.
12 V. K. Garg, M. Amita, R. Kumar and R. Gupta, *Dyes Pigm.*, 2004, **63**, 243–250.
13 S. Khan, A. Wong, M. V. B. Zanoni and M. D. P. T. Sotomayor, *Mater. Sci. Eng., C*, 2019, **103**, 109825.
14 X. Yu, H. Liu, J. Diao, Y. Sun and Y. Wang, *Sep. Purif. Technol.*, 2018, **204**, 213–219.
15 H. Gao, S. Zhao, X. Cheng, X. Wang and L. Zheng, *Chem. Eng. J.*, 2013, **223**, 84–90.
16 M. A. M. Salleh, D. K. Mahmoud, W. A. W. A. Karim and A. Idris, *Desalination*, 2011, **280**, 1–13.
17 E. Sterenzon, V. K. Vadivel, Y. Gerchman, T. Luxbacher, R. Narayanan and H. Mamane, *ACS Omega*, 2022, **7**, 118–128.
18 M. Anbia and S. Salehi, *Dyes Pigm.*, 2012, **94**, 1–9.
19 S. Ahmadi, L. Mohammadi, A. Rahdar, S. Rahdar, R. Dehghani, C. A. Igwegbe and G. Z. Kyzas, *Nanomaterials*, 2020, **10**, 556.
20 T. Robinson, G. McMullan, R. Marchant and P. Nigam, *Bioresour. Technol.*, 2001, **77**, 247–255.

21 W. Li, Q. Yue, P. Tu, Z. Ma, B. Gao, J. Li and X. Xu, *Chem. Eng. J.*, 2011, **178**, 197–203.

22 G. Crin, *Bioresour. Technol.*, 2006, **97**, 1061–1085.

23 C. Namasivayam and D. Kavitha, *Dyes Pigm.*, 2002, **54**, 47–58.

24 B. H. Hameed, A. T. M. Din and A. L. Ahmad, *J. Hazard. Mater.*, 2007, **141**, 819–825.

25 Z. Long, Y. Lu, M. Zhang and H. Qiu, *J. Sep. Sci.*, 2014, **37**, 2764–2770.

26 S. A. Zaidi, *Crit. Rev. Anal. Chem.*, 2019, **49**, 324–335.

27 J. Yao, X. Li and W. Qin, *Anal. Chim. Acta*, 2008, **610**, 282–288.

28 K. Sreenivasan, *J. Appl. Polym. Sci.*, 1999, **71**, 1819–1821.

29 H. F. Hawari, N. M. Samsudin, M. N. Ahmad, A. Y. M. Shakaff, S. A. Ghani, Y. Wahab, S. K. Za'aba and T. Akitsu, *Procedia Chem.*, 2012, **6**, 100–109.

30 F. Lanza and B. Sellergren, *Anal. Chem.*, 1999, **71**, 2092–2096.

31 G. Li and K. H. Row, *Sep. Purif. Rev.*, 2018, **47**, 1–18.

32 D. Spivak, M. A. Gilmore and K. J. Shea, *J. Am. Chem. Soc.*, 1997, **119**, 4388–4393.

33 T. Shiomi, M. Matsui, F. Mizukami and K. Sakaguchi, *Biomaterials*, 2005, **26**, 5564–5571.

34 S. S. Arani, S. J. Ahmadi, A. B. Samani and M. G. Maragheh, *Anal. Chim. Acta*, 2008, **623**, 82–88.

35 A. Murray and B. Ormeci, *Environ. Sci. Pollut. Res.*, 2012, **19**, 3820–3830.

36 A. H. Wu and M. J. Syu, *Biosens. Bioelectron.*, 2006, **21**, 2345–2353.

37 C. Zheng, Y. P. Huang and Z. S. Liu, *J. Sep. Sci.*, 2011, **34**, 1988–2002.

38 A. R. Koohpaei, S. J. Shahtaheri, M. R. Ganjali, A. R. Forushani and F. Golbabaei, *Talanta*, 2008, **75**, 978–986.

39 X. Luo, Y. Zhan, Y. Huang, L. Yang, X. Tu and S. Luo, *J. Hazard. Mater.*, 2011, **187**, 274–282.

40 S. Lay, X. Ni, H. Yu and S. Shen, *J. Sep. Sci.*, 2016, **39**, 2321–2331.

41 A. Mirmohseni, R. Pourata and M. Shojaei, *IEEE Sens. J.*, 2014, **14**, 2807–2812.

42 W. J. Cheong, S. H. Yang and F. Ali, *J. Sep. Sci.*, 2013, **36**, 609–628.

43 W. J. Cheong, F. Ali, J. H. Choi, J. O. Lee and K. Y. Sung, *Talanta*, 2013, **106**, 45–59.

44 Z. M. Li, J. M. Liu, Z. B. Liu, Q. Y. Liu, X. Lin, F. M. Li, M. L. Yang, G. H. Zhu and X. M. Huang, *Anal. Chim. Acta*, 2007, **589**, 44–50.

45 Y. P. Song, N. Li, H. C. Zhang, G. N. Wang, J. X. Liu, J. Liu and J. P. Wang, *Food Chem.*, 2017, **233**, 422–428.

46 J. Jiang, K. Song, Z. Chen, Q. Zhou, Y. Tang, F. Gu, X. Zuo and Z. Xu, *J. Chromatogr. A*, 2011, **1218**, 3763–3770.

47 E. Piletska, S. Piletsky, K. Karim, E. Terpetschnig and A. Turner, *Anal. Chim. Acta*, 2004, **504**, 179–183.

48 F. Ali, W. J. Cheong, A. Rafique, Z. A. AlOthman, M. Sadia and M. Muhammad, *J. Sep. Sci.*, 2021, **44**, 1430–1439.

49 F. Ali, A. R. Malik, W. J. Cheong and N. U. Rehman, *J. Liq. Chromatogr. Relat.*, 2019, **42**, 662–672.

50 N. Arabzadeh, A. Khosravi, A. Mohammadi, N. M. Mahmoodi and M. Khorasani, *Desalin. Water Treat.*, 2015, **54**, 2452–2460.

51 Z. Long, Y. Lu, M. Zhang and H. Qiu, *J. Sep. Sci.*, 2014, **37**, 2764–2770.

52 M. L. Quinto, S. Khan, G. Picasso and M. D. P. T. Sotomayor, *J. Hazard. Mater.*, 2020, **384**, 121374.

53 X. Luo, Y. Zhan, Y. Huang, L. Yang, X. Tu and S. Luo, *J. Hazard. Mater.*, 2011, **187**, 274–282.

54 X. Yu, H. Liu, J. Diao, Y. Sun and Y. Wang, *Sep. Purif. Technol.*, 2018, **204**, 213–219.

55 A. K. Mishra, T. Arockiadoss and S. Ramaprabhu, *Chem. Eng. J.*, 2010, **162**, 1026–1034.

56 G. Li and K. H. Row, *Sep. Purif. Rev.*, 2018, **47**, 1–18.

57 T. T. Win, T. M. Swe, H. H. Ei, N. N. Win, K. Kyi Swe, W. Nandar, T. k. Ko and P. Fu, *Biodegradation*, 2021, **32**, 697–710.

58 S. Agrawal, D. Tipre, B. Patel and S. Dave, *Process Biochem.*, 2014, **49**, 110–119.

59 V. K. Garg, M. Amita, R. Kumar and R. Gupta, *Dyes Pigm.*, 2004, **63**, 243–250.

60 A. H. Wu and M. J. Syu, *Biosens. Bioelectron.*, 2006, **21**, 2345–2353.

61 A. Murray and B. Ormeci, *Environ. Sci. Pollut. Res.*, 2012, **19**, 3820–3830.

62 M. A. M. Salleh, D. K. Mahmoud, W. A. W. A. Karim and A. Idris, *Desalination*, 2011, **280**, 1–13.

63 A. Gurses, C. Dogar, M. Yalcin, M. Acıkıldız, R. Bayrak and S. Karaca, *J. Hazard. Mater.*, 2006, **131**, 217–228.

64 B. H. Hameed, A. T. M. Din and A. L. Ahmad, *J. Hazard. Mater.*, 2007, **141**, 819–825.

65 C. Namasivayam and D. Kavitha, *Dyes Pigm.*, 2002, **54**, 47–58.

66 Y. C. Sharma and F. J. Uma Gode, *Chem. Eng. Data*, 2010, **55**, 3991.

67 T. S. Singh and K. K. Pant, *Sep. Purif. Technol.*, 2004, **36**, 139–147.

68 K. Mosher, J. He, Y. Liu, E. Rupp and J. Wilcox, *Int. J. Coal Geol.*, 2013, **109**, 36–44.

69 W. J. Weber and J. C. Morris, *J. Sanit. Eng. Div.*, 1963, **89**, 31–60.

70 W. Zhang, Q. Li, J. Cong, B. Wei and S. Wang, *Polymers*, 2018, **10**, 216.

71 G. F. Abu-Alsoud, K. A. Hawboldt and C. S. Bottaro, *ACS Appl. Mater. Interfaces*, 2020, **12**, 11998–12009.

72 G. McKay, H. S. Blair and J. R. Gardner, *J. Appl. Polym. Sci.*, 1982, **27**, 3043–3057.

73 R. A. Latour, *J. Biomed. Mater. Res.*, 2015, **103**, 949–958.

74 L. X. Xia, Z. Shen, T. Vargas, W. J. Sun, R. M. Ruan, Z. D Xie and G. Z. Qiu, *Biotechnol. Lett.*, 2013, **35**, 2129–2136.

75 A. Ozer and H. B. Pirinc, *J. Hazard. Mater.*, 2006, **137**, 849–855.

76 A. O. O. Dada, A. P. Olatunya and A. M. DADA, Langmuir, Freundlich, Temkin and Dubinin–Radushkevich, *J. Appl. Chem.*, 2012, **3**, 38–45.

77 Y. Q. Xia, T. Y. Guo, M. D. Song, B. H. Zhang and B. Zhang, *React. Funct. Polym.*, 2006, **66**, 1734–1740.

78 Y. Liu, L. Wu, X. Zhao and A. Luo, *Int. J. Polym. Anal.*, 2012, **17**, 38–47.

79 M. B. Desta, *J. Chem. Thermodyn.*, 2013, 375830.

80 M. Kucharska and J. Grabka, *Talanta*, 2010, **80**, 1045–1051.

81 N. Vachirapatama, J. Mahajaroensiri and W. Visessanguan, *J. Food Drug Anal.*, 2008, **16**, 77–82.